Environmental Science and Pollution Research (2023) 30:124992–125005
https://doi.org/10.1007/s11356-023-28782-5

CARBON-BASED NANOMATERIALS: SYSTEMATIC ENUMERATION AND PROFICIENT TEMPLATE FOR DETECTION AND REMEDIATION OF HAZARDOUS POLLUTANTS

Improved photocatalytic decolorization of reactive black 5 dye through synthesis of graphene quantum dots–nitrogen-doped TiO_2

Muhammad Saqib Khan[1,2] · Nadia Riaz[1] · Saeed Rehman[3] · Liu Chenhui[3] · Ahson Jabbar Shaikh[4] · Muhammad Arfan[5] · Iftikhar Zeb[6] · Muhammad Arshad[7] · Farhan Hafeez[1] · Muhammad Bilal[1]

Received: 30 September 2022 / Accepted: 10 July 2023 / Published online: 27 July 2023

Abstract
Graphene quantum dots (GQDs), a new solid-state electron transfer material was anchored to nitrogen-doped TiO_2 via sol gel method. The introduction of GQDs effectively extended light absorption of TiO_2 from UV to visible region. GQD-N-TiO_2 demonstrated lower PL intensity at excitation wavelengths of 320 to 450 nm confirming enhanced exciton lifespan. GQD-N-TiO_2-300 revealed higher surface area (191.91m^2 g^{-1}), pore diameter (1.94 nm), TEM particle size distribution (4.88 ± 1.26 nm) with lattice spacing of 0.45 nm and bandgap (2.91 eV). In addition, GQDs incorporation shifted XPS spectrum of Ti 2p to lower binding energy level (458.36 eV), while substitution of oxygen sites in TiO_2 lattice by carbon were confirmed through deconvolution of C 1 s spectrum. Photocatalytic reaction followed the pseudo first order reaction and continuous reductions in apparent rate constant (K_{app}) with incremental increase in RB5 concentration. Langmuir–Hinshelwood model showed surface reaction rate constants $K_C = 1.95$ mg L^{-1} min^{-1} and $K_{LH} = 0.76$ L mg^{-1}. The active species trapping, and mechanism studies indicated the photocatalytic decolorization of RB5 through GQD-N-TiO_2 was governed by type II heterojunction. Overall, the photodecolorization reactions were triggered by the formation of holes and reactive oxygen species. The presence of •OH, $^1O_2$, and O_2• during the photocatalytic process were confirmed through EPR analysis. The excellent photocatalytic decolorization of the synthesized nanocomposite against RB5 can be ascribed to the presence of GQDs in the TiO_2 lattice that acted as excellent electron transporter and photosensitizer. This study provides a basis for using nonmetal, abundant, and benign materials like graphene quantum dots to enhance the TiO_2 photocatalytic efficiency, opening new possibilities for environmental applications.

Keywords Graphene quantum dots · Photosensitizer · Heterogeneous reaction · Reaction kinetics · Type II heterojunction

Introduction

The broad applicability and better performance of heterogenous photocatalytic reactions driven by visible light offer a viable solution to the rapidly increasing environmental challenges of toxic organic colorants (Yang et al. 2021). The interest in designing and improving the photocatalysts for an increased visible light–driven decolorization of dyes has augmented around the world (Iftikhar et al. 2020). Titanium dioxide (TiO_2) is undeniably one of the most widely investigated photocatalysts, due to its effective oxidizing power, superior photostability, relatively high photocatalytic activity, low cost, and toxicity, providing a simple and economical alternative for decolorization of environmental pollutants (Khan et al. 2021a; Riaz et al. 2021, 2014). Despite their good performances and durability, the poor

Responsible Editor: Sami Rtimi

Highlights

• GQDs were anchored to nitrogen-doped $TiO_2$for enhanced photocatalytic activity
• Physicochemical properties were improved throughdecoration of GQDs
• Exciton lifetime increased with GQDs decorationon nitrogen-doped TiO_2
• Type II heterojunction was proposed for photocatalyticdecolorization by GQD-N-TiO_2
• Photodecolorization reactions were triggered byholes and reactive oxygen species

Extended author information available on the last page of the article

response to visible light–induced by TiO_2's large bandgap, as well as the quick recombination of photogenerated electron–hole pairs, have limited the use of pristine TiO_2 in photocatalytic processes (Miodyńska et al. 2020). Hence, many research groups have studied different techniques to broaden the absorption spectrum and improve the photo response of TiO_2, including heteroatom doping (Cheng et al. 2020; Riaz et al. 2012), sensitizing TiO_2 with lower bandgap semiconductors (Pourzad et al. 2020; Upadhyay et al. 2020), and most recently coupling with quantum dots (QDs) (Khan et al. 2021b; Miranda-Andrades et al. 2020). Among these strategies, metal free materials for instance carbon/nitrogen, have been claimed as the best alternative to restrain electron and hole recombination rate for better photocatalytic performance (Koe et al. 2020). Substitutional doping of nitrogen in TiO_2 has been considered effective in reducing the bandgap (Pourzad et al. 2020). Our research group reported the photocatalytic and biocidal application of N–TiO_2 and among different combination 20 mol percent nitrogen in TiO_2 (20N–TiO_2) calcined at 300 °C depicted reduced bandgap, i.e., 2.95 eV (Khan et al. 2020). Zhou and coworkers recently reported that the O 2p and N 2p states right above the VB can merge synergistically when N is added to the TiO_2 lattice, reducing the bandgap and increasing the visible light sensitivity of TiO_2 (Zhou et al. 2020). Thus, combining TiO_2 with nitrogen to create defect rich heterostructures is a promising technique to enhance photocatalytic activity.

In addition, several advantages arise in defect mediated heterostructures, including numerous active sites, improved redox efficiency, and enhanced visible light response. It is noticeable that small defects from introduction of carbon and nitrogen-doped TiO_2 have resulted in improved photocatalytic performance (Li et al. 2012); however, less attention has been made at the impact of bigger defects. Semiconductor nanocrystals also known as QDs have been investigated as bigger defects to absorb photon for efficient solar energy conversion. Due to the tunable bandgap and multiple excitons, TiO_2-sensitized QDs like CdS (Sadhasivam et al. 2021) and CdSe (Kang et al. 2021) have gained a lot of interest. Although the photo response of TiO_2 can be effectively improved with these materials; however, the limiting factor associated with these types of materials is their instability to hole oxidation in aqueous medium subsequently damaging the heterojunctions, leading to poor performance. Moreover, photo-oxidation releases highly toxic Cd ions into the solution, thus making the utilization of conventional heterojunctions unsafe and undesirable to the environment.

Recently, a new type of QDs materials, GQDs has attracted a lot of attention due to their plethora and desirable physicochemical properties like excellent solubility, chemical inertness, stable photoluminescence, biocompatibility, and environmental friendliness. Moreover, wide range of potential applications like solar cells (Mahalingam et al. 2021), bioimaging (Gómez et al. 2021; Shah et al. 2021), light-emitting devices (Yoon et al. 2020), biosensing (Bruce & Clapper 2020), and photocatalysis (Chen et al. 2020; Khan et al. 2021b) makes them prominent among other semiconductors. GQDs, compared to other conventional semiconductor QDs, are non-toxic and very resistant to various chemical conditions. Furthermore, GQDs maintain graphene structure with a larger surface area and stable sp^2 bonding without extra passivation to get rid of surface traps, with the exception of edge sites. Moreover, the tunable electronic configuration of GQDs in wide energy range allows them to construct different heterojunctions. Beside all the abovementioned advantages, pristine GQDs exhibited lower catalytic activity due to the faster electrons and holes recombination. Thus, doping GQDs with other materials/semiconductors is effective to tune the electronic structure for photocatalytic applications. In recent years, GQDs have been used to develop photocatalysts with enhanced photocatalytic properties by combining them with other semiconductors as a potential energy–transfer component, these include ZnSe (Lei et al. 2021), ZnCdS (Jiang et al. 2020), ZnO (Wu et al. 2020), Fe_3O_4 (Ganganboina et al. 2017), SiO_2 (Chang et al. 2021), and TiO_2 (Albargi et al. 2021; Guo et al. 2020). Zheng et al. synthesized SN-GQDs/TiO_2 through hydrothermal and impregnation method for photocatalytic H_2O_2 production (451 μmol L^{-1}) (Zheng et al. 2018). Guo et al. constructed the p–n junction P-GQD-TiO_2 nanocomposite through hydrothermal technique for the photodegradation of methyl orange (95%) (Guo et al. 2020). Albargi et al. fabricated UV photodetector using TiO_2 and N-GQDs bilayer heterojunction on SiO_2 having higher absorption and efficient transport mechanism (Albargi et al. 2021). Khorshidi et al. revealed that using TiO_2 nanorods as an electron transport layer in perovskite solar cells fabricated using a one-step hydrothermal technique enhanced power conversion efficiency by 217% than mesoporous TiO_2, whereas GQDs-TiO_2 had a 1.34 times greater efficiency than TiO_2 nanorods (Khorshidi et al. 2020). Furthermore, Sun et al. indicated that the NGQDs/TiO_2 (P25) composites developed via hydrothermal method had better photocatalytic activity due to better photon absorption capacity and improved electron–hole transfer (Sun et al. 2019). Despite various reports of TiO_2-based visible light–driven photocatalysts coupled to GQDs, the poor quantum yield and complex process parameters of GQDs still necessitates the use of alternate technologies and materials. Furthermore, investigations into the characteristics and mechanisms of photocatalysis of GQD–N–TiO_2 composites with high photocatalytic activity is still desired.

Herein, we reported the one-step sol gel process for the synthesis of GQD-doped nitrogen-doped TiO_2 with improved physicochemical properties. The synthesized nanocomposite was tested against a model pollutant from textile industry, reactive black 5 (RB5), an anionic double azo dye. The anionic RB5 is due to the sulfonated group in the dye structure. The presence of dyes in wastewater and soil poses mutagenic and carcinogenic threats to living organisms. Therefore, it is essential to treat such dyes before their release into the freshwater system. On the RB5 decolorization, the properties and enhanced photocatalytic activity of composites with various GQD weight contents were studied while the nitrogen contents optimization were reported in our previous finding (Khan et al. 2020). The novelty of this work lies in the synthesis of a new solid-state electron transfer material, i.e., graphene quantum dots and their anchoring to nitrogen-doped TiO_2 using the sol–gel method. The introduction of GQDs with nitrogen extends the light absorption of TiO_2 from UV to visible region, resulting in lower photoluminescence intensity and longer exciton lifespan. The study also provides a promising approach for using graphene quantum dots as a nonmetal, abundant, and benign material to enhance the photocatalytic efficiency of TiO_2, opening new possibilities for environmental applications.

Experimental section

GQDs synthesis

GQDs were synthesized by direct pyrolysis of citric acid (CA) (Dong et al. 2012) with a little modification. CA was pyrolyzed for 5 min at 200℃ on a heating mantle. The GQDs development was observed when the color changed to orange. The obtained orange solution was treated with ethanol containing 10 mg mL^{-1} NaOH. The obtained liquid GQDs were further used to synthesize the final composite material.

Synthesis of GQD–20N–TiO_2 nanocomposite

A 20 mol% nitrogen (20N–TiO_2) was selected to synthesize GQD–20N–TiO_2 (Khan et al. 2020). In a typical sol–gel approach GQD–20N–TiO_2 gel was obtained by thoroughly mixing titania precursor (TTIP), GQD solution ("GQDs synthesis"), desired amount of nitrogen precursor (urea) in absolute ethanol at ambient conditions under vigorous stirring. The synthesized gel was kept for aging overnight followed by drying at 90℃ overnight in an oven. The raw GQD–20N–TiO_2 was ground to powder and calcined at 300℃ for 1 h.

Characterization of the photocatalysts

The synthesized nanocomposites were characterized using, X-ray diffraction, UV visible spectrophotometer, Fourier-transform infrared spectroscopy, scanning electron microscopy, (SEM), high-resolution transmission electron microscope (HRTEM), Brunauer–Emmett–Teller analysis (BET), and X-ray photoelectron spectrometer (XPS).

Photocatalytic reaction studies

Using the photocatalytic experiment setup from our previous investigation (Khan et al. 2021c), the decolorization studies were performed at working pH, ambient temperature, and initial RB5 concentration (30 mg L^{-1}). Prior to the photocatalytic reaction, the nanocomposite (1 mg mL^{-1}) was dispersed in distilled water and RB5 dye was added to this dispersed solution to achieve the final concentration of 30 mg L^{-1}. In a typical batch reaction, the suspension was continuously stirred on a stirring plate at 200 rpm for 30 min without light (dark reaction), followed by 1 h in visible light at 25 cm. The light source was halogen lamp (30,798 lx). The RB5 decolorization was monitored in the aliquots collected at different time intervals through UV–Vis spectrophotometer (PG instruments UK, model T80^{+}) at 598 nm. The following expression was used to determine the decolorization efficiency, (Eq. 1).

$$\text{RB5 decolorization (\%)}=\left(\frac{C_0 - C_t}{C_0}\right)100 \tag{1}$$

Where C_0 is initial RB concentration, and C_t is the RB5 concentration at time, t.

The photostability of the dye was monitored through control experiment in presence of light and without nanocomposite. Prior to absorbance measurements, a calibration curve was obtained with known RB5 concentrations (0, 1, 10, 20, 30, 50, 60, and 100 mg L^{-1}). Effects of various reaction parameters including irradiation time, nanocomposite amount, pH, and initial dye concentration were performed for the best performing photocatalyst. The photocatalytic reaction was modeled through Langmuir–Hinshelwood (L–H) isotherm (Eq. 2)

$$\frac{1}{k_{app}} = \frac{1}{K_c}[\text{RB5}]_e + \frac{1}{K_c K_{ads}} \tag{2}$$

Slope is $1/k_c$ and intercept $1/k_c K_{ads}$ in the plot of $1/k_{app}$ versus equilibrium concentration. The L–H model is expressed in linear form in the following equation for the explanation of initial [RB5] effect on initial rate (r_0), (Eq. 3).

$$\frac{1}{r_0} = \frac{1}{K_c} + \frac{1}{K_c K_{ads}} \cdot \frac{1}{[RB5]_e} \quad (3)$$

Reusability studies

Reusability studies were conducted to check the stability of the synthesized photocatalysts for different cycles. The used-photocatalysts were collected through centrifugation and washed with distilled water. The collected photocatalysts were dried and utilized again under the same experimental conditions.

Electrical energy consumption studies

The following equation was used to calculate the energy efficiency of GQD–20N–TiO_2–300 photocatalysts based on their electrical energy consumption (EE/O), Eq. (4). (Azbar et al. 2004).

$$E_{E/O} = \frac{(pt)1000}{[(V)60\ \ln\left(\frac{C_0}{C_f}\right)} \quad (4)$$

Results and discussion

Characterization of the photocatalysts

The functional groups of the synthesized nanoparticles were identified using FTIR analysis. Figure 1a depicted the stretching vibrations of Ti–O–Ti in the IR range of 500–900 cm^{-1} while a very minor peak at around 1040 cm^{-1} in GQD–20N–TiO_2 nanocomposite may have been caused by Ti–O–N. The interaction between nitrogen and titania in the GQD–N–TiO_2 nanocomposite, which revealed –N-O_x (Ti–O–N–Ti) in a small band at 1380 cm^{-1}, further supports the existence of nitrogen.(Azami et al. 2017), and a small peak at 1650 cm^{-1} was assigned to C—N stretching (Factorovich et al. 2011). Intermolecular forces of hydroxyl group in the nanocomposite are shown by broad peaks at 3100 cm^{-1}, and sharp peak around 1530 cm^{-1} indicating water presence at the particle surface for the synthesized nanocomposites (Khan et al. 2020).

Figure 1b shows the XRD diffraction pattern of TiO_2, and GQDs and nitrogen co-doped TiO_2 photocatalysts calcined at 300 °C. The GQD–20N–TiO_2-300 showed a wide peak at about 26°, which corresponds to the (002) diffraction planes of graphite carbon (Martins et al. 2016). The broadening of this peak is associated with the nano-size of GQDs in GQD–20N–TiO_2-300 (Mahato et al. 2021). Moreover, both samples TiO_2–300 and GQD–20N–TiO_2–300 showed diffraction peaks at 25.4°, 38.1°, 48.1°, 54.7°, 55.59°, 62.8°, 68.8°, 70.4°, and 75.1° corresponding to (101), (004), (200), (105), (211), (204), (220), (116), and (215) confirming tetragonal TiO_2 (anatase) (Shabir et al. 2021). The crystalline structure of TiO_2-300 and GQD–20N–TiO_2-300 was fairly maintained due to the small fraction and the proper dispersion of the GQDs in TiO_2 (Mahato et al. 2021). The anatase crystallite sizes and relative crystallinity of the synthesized photocatalysts were determined through Scherrer formula. The crystallite size of TiO_2, and GQD–20N–TiO_2-300 was 36, and 7.37 nm with relative percent crystallinity of 75.72 and 69.24, respectively.

The absorbance spectra of TiO_2-300 photocatalysts (Fig. 1c) revealed a strong absorption edge around 390 nm, with almost no visible light absorption, while a sharp red shift was observed upon introducing nonmetal entities. In our previous study, a marginal red shift was observed with nitrogen doping (Khan et al. 2020); however, the visible light absorption is enhanced with GQDs loading in the current study. The change in bandgap energy (E_g) from the UV region for TiO_2–300 to the visible region for GQDs loaded TiO_2 can be seen by carefully observing the Tauc`s plot (Fig. 1d). The estimated E_g for TiO_2-300 and GQD–20N–TiO_2-300 were 3.19 and 2.91 eV, respectively, this gradual decrease in E_g is attributed to the free electron properties in the conduction band; moreover, this trend also confirms the structural changes in the TiO_2 matrix upon doping (Khore et al. 2018).

The addition of GQDs to TiO_2-300 resulted in improved surface properties, as confirmed by the BET surface area analysis (Fig. 1e). Both the TiO_2-300 and GQDs-doped TiO_2 samples exhibited a type IV BET isotherm with an H_3 hysteresis loop. This indicates a gradual adsorption of multiple layers of gas, suggesting the presence of well-defined mesoporous surfaces with a relatively narrow size distribution. The surface area for TiO_2–300 and GQD–20N–TiO_2–300 was 66.31 and 191.91$m^2\ g^{-1}$, respectively, while the pore diameter decreased from 6.85 to 1.94 nm. The absence of a distinct monolayer formation implies that the adsorption process occurs gradually without a sharp transition. The H_3 hysteresis loop, appearing in the multilayer range of physisorption isotherms, is characteristic of aggregates of plate-like particles, which give rise to slit-shaped pores within the material. This information highlights the presence of well-defined mesoporous structures in the samples, providing insight into the surface properties and pore characteristics of the material. Previous studies (Khan et al. 2020) support these observations, as they demonstrated that 20N–TiO_2–300 without the inclusion of GQDs exhibited a lower surface area of 49.54 $m^2\ g^{-1}$ and a higher pore diameter of 21.3 nm. Thus, the introduction of GQDs into *N*-doped TiO_2 led to an increase in surface area, which can be attributed to the unique physical and chemical properties of GQDs and may contain many active sites that can interact with the

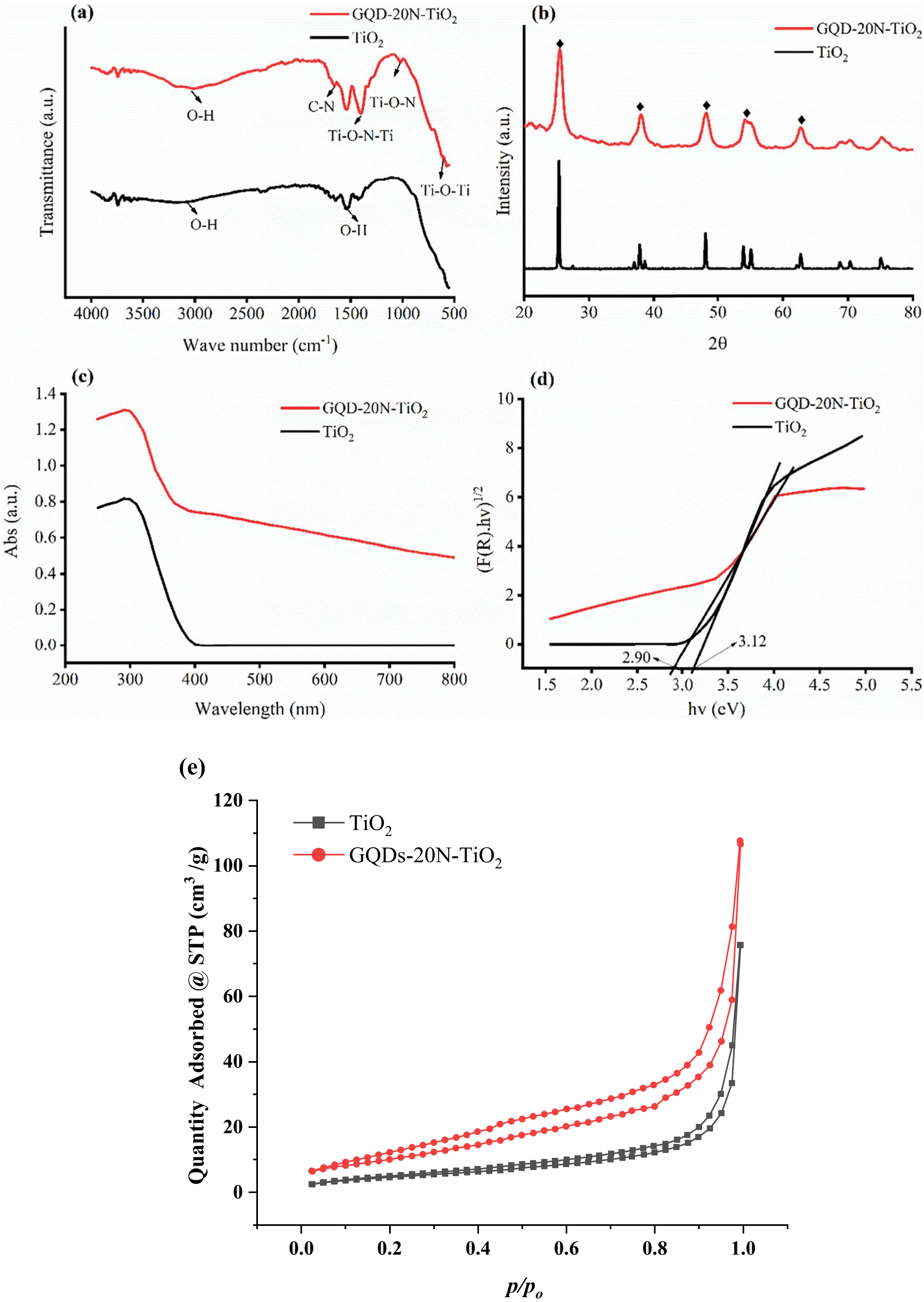

Fig. 1 Physicochemical analysis of TiO_2, and GQDs-20N-TiO_2 calcined at 300 °C (**a**) FTIR, (**b**) XRD, (**c**) absorption spectrum (**d**) Tauc's plot, (**e**) N_2 adsorption/desorption isotherms

TiO_2 surface, leading to the development of controlled pore structure. This increased porosity is advantageous resulting an increase in the surface area of the material. In addition, consequently, a number of photoactive sites can be provided by the porous GQD–20N–TiO_2–300 nanocomposite which ultimately increase the photocatalytic activity.

Figure 2 shows SEM micrographs of TiO_2, and GQD–20N–TiO_2 calcined at 300 °C. The GQD–20N–TiO_2 clearly shows distinctive carbon framework having irregular arrangements and dispersion. Previous study reported uneven distribution and partial coating in carbon-doped TiO_2, suggesting a TiO_2 to carbon ratio of 2:1 (Peñas-Garzón et al. 2021); however, in our case, this ratio was 9:1, that might be the reason of irregular morphology in GQD–20N–TiO_2. Similar results were reported in case of GQD decorated iron-doped TiO_2 (Khan et al. 2021b). In our recent work, we found that TiO_2 and 20N-TiO_2 had similar morphology, with a regular spherical shape (Khan et al. 2020). The mean particle size estimated was 65, and 28 nm for TiO_2, and GQD–20N–TiO_2. To acquire better understanding of the morphology of the synthesized nanocomposite, TEM micrographs are depicted in Fig. 3a and b. Figure 3a-i and b-i reveals a uniform size distribution without clear aggregation with an average particle size 4.54 ± 0.54 nm and 4.88 ± 1.26 nm (Fig. 3a-iii and b-iii) for TiO_2, and GQD–20N–TiO_2, respectively. Figure 3a-ii and b-ii depicted the lattice spacing is about 0.45 nm. Furthermore, the lattice fringes observed in the HRTEM images indicate the crystal lattice of the material. In graphene quantum dots–doped N-TiO_2, the lattice fringes may indicate both the anatase TiO_2 and the graphene quantum dots, as they are both present in the nanocomposite. The XRD pattern also showed the crystal structure of the nanocomposite, including the anatase TiO_2 phase, but it may not show the presence of graphene quantum dots, as they may not contribute significantly to the XRD pattern due to their small size and low crystallinity. It is possible for a material to have both nano- and semi-crystalline nature, which could explain the high crystallinity observed in the HRTEM images despite the nano-sized crystals observed in the XRD pattern.

The photo luminance (PL) technique was used to investigate the efficacy of electron and holes transfer, trapping, and recombination rate. The PL is caused by the recombination of electrons and holes, and the rate of recombination is related to the PL intensity (Khan et al. 2021b; Stankovich et al. 2006), the lower the PL intensity, the lower shall be the charge recombination. Figure 4 depicted the PL spectra of the synthesized photocatalysts. A broad peak around 375, 417, and 420 nm with high emission can be seen for TiO_2, 20N–TiO_2, and GQD–20N–TiO_2 respectively. When impurities were introduced into TiO_2, the PL intensity is substantially reduced, indicating elongation of the e^-/h^+ pairs lifespan. Charge recombination is reduced by the formation of a Schottky barrier at the GQD and 20N-TiO_2 interface. Furthermore, GQDs have impact on trapping electrons from the TiO_2 surface, avoiding rapid charge recombination and improving photocatalytic performance. The E_g obtained from the PL spectra (inset Fig. 4) were 3.30, 2.95, and 2.98 eV for TiO_2, 20N-TiO_2, and GQD–20N–TiO_2 respectively.

Figure 5a–e illustrates the XPS survey of the synthesized nanocomposite, i.e., GQD–20N–TiO_2-300. Strong signal of

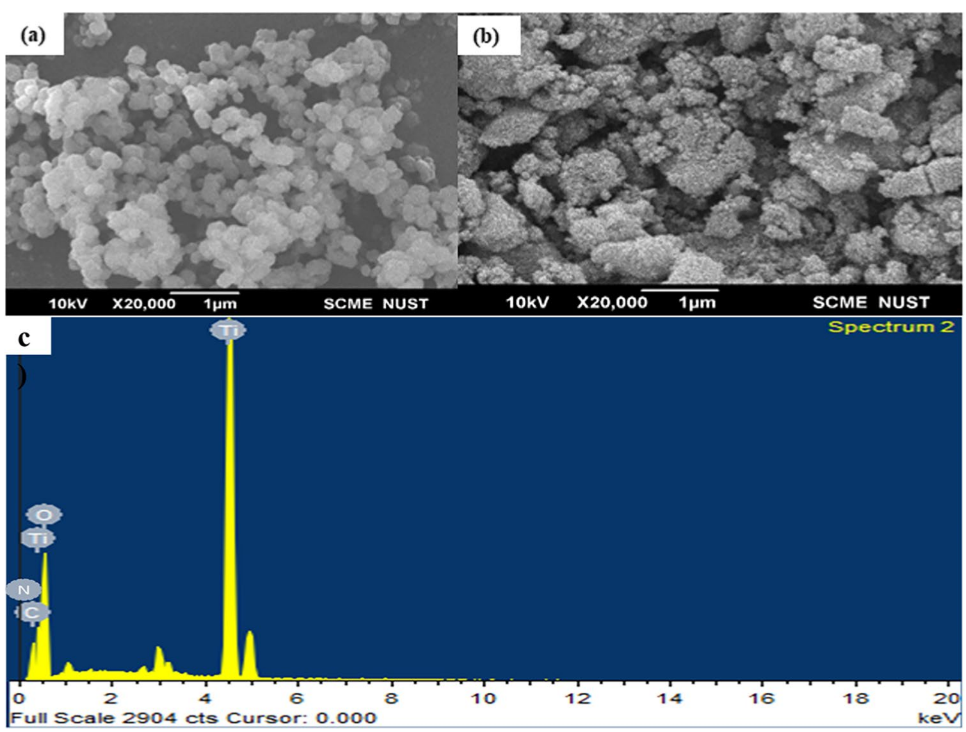

Fig. 2 SEM images of (**a**) TiO_2, (**b**) GQD–20N–TiO_2 and (**c**) EDX profile of GQD–20N–TiO2 calcined at 300 °C

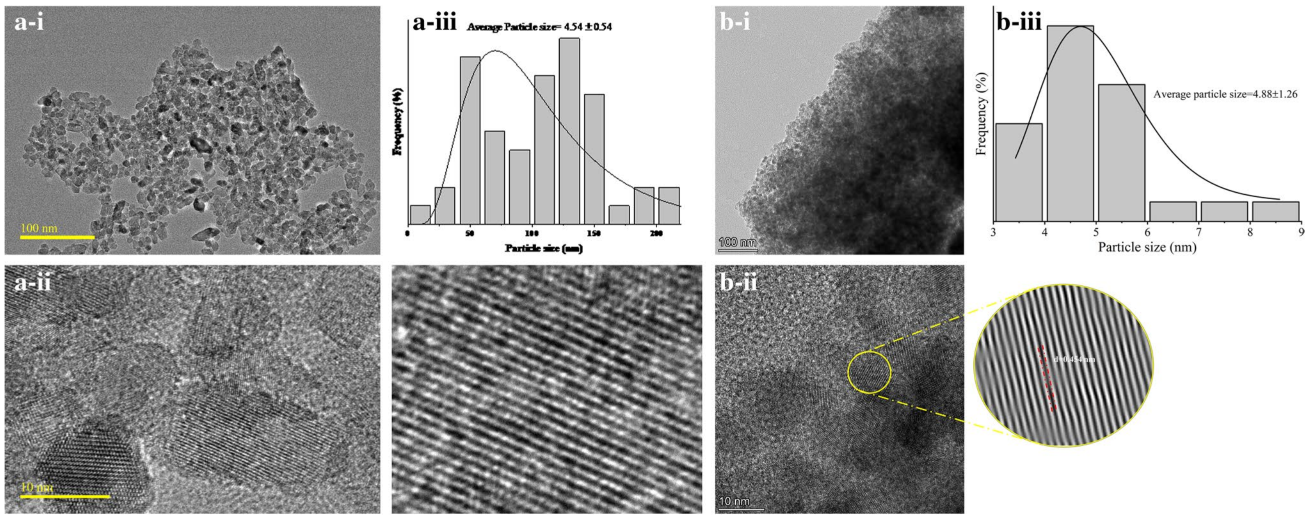

Fig. 3 TEM images of **a** bare TiO_2 and **b** GQD–20N–TiO_2-300 (i) simplified illustrative nanostructure of GQD–20N–TiO_2-300, (ii) the HRTEM image of with measured lattice spacing, and (iii) lateral size distribution

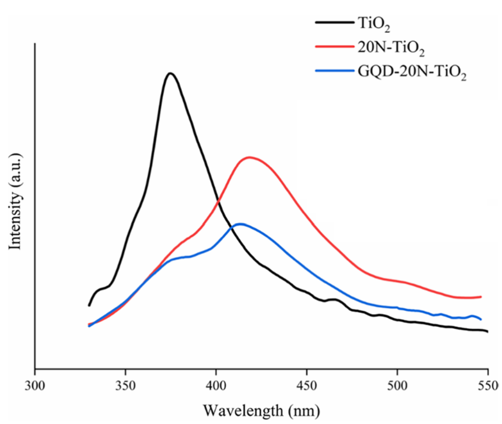

Fig. 4 PL spectra of TiO_2, 20N-TiO_2, and GQD–20N–TiO_2 calcined at 300 °C

Ti 2p, C 1 s, and O 1 s were observed while weak signals of N 1 s confirms the nitrogen doping in the composite. High-resolution Ti 2p spectrum depicted the binding energy peaks at 458.36 and 464.17 eV of Ti $2p_{3/2}$ and Ti $2p_{1/2}$, respectively (Pan et al. 2015). The low-binding energy of Ti 2p in co-doped TiO_2 indicates that Ti interacts with ions and replaced in a different way. In literature, the XPS peak of Ti 2p normally appears at 259.5 eV in pristine TiO_2 (Saha & Tompkins 1992), while nitrogen-doped TiO_2 appears at 459.2 eV (Abdullah et al. 2016); however, in our study, the GQDs incorporation shifted the XPS spectrum to lower binding energy level (458.36 eV). The broadness of peak in the Ti 2p spectrum was attributed to the central photoemission–related energy loss process, extrinsic, and/or intrinsic. Studies reported that extrinsic effects occurs when photoelectrons traverses to the surface, resulting in energy loss due to plasma excitation while valence electron excitations within the photoemitting atom is assumed to cause the intrinsic effects (Chambers 2016). The deconvolution of the high-resolution C 1 s spectrum reveals the strong signals at 284.73, 285.91, and 288.50 eV corresponding to the formation of C–C─sp^2, N─sp^2C, and N─sp^3C (Xue et al. 2016), indicating the substitution of oxygen sites in TiO_2 lattice by carbon. The formation of these interactions confirms the results obtained in PL and DRS analysis where exciton life is elongated through reduction in bandgap. Furthermore, the N 1 s spectrum revealed three peaks at 399.05, 400.01, and 401.92 eV which assigned, respectively, to N─C, Ti─N─O, and -NH_2, attributed to the bonding of nitrogen with GQD and TiO_2. Ti─O peaks were recorded in O 1 s high-resolution spectrum at 529.60 eV (Lu et al. 2014). These XPS findings agree with the other characterization results, indicating the presence and binding of nitrogen with Ti and GQDs in the composite.

Effect of GQDs content

Figure 6a shows the effect of different GQDs weight percent (0.2, 0.5, 1, 1.5, 2.0, 2.5, 3.0, and 5.0) on RB5 decolorization for 30 min photocatalytic reaction. The photocatalytic activity decreased with increasing GQDs contents, as higher GQD content forms a thick layer that prevents photons from reaching the TiO_2 surface, resulting in decreased photocatalytic activity (Pan et al. 2015). Several reports proposed that GQDs-TiO_2 composites provide excellent photocatalytic activity due to the interaction between GQDs and TiO_2 nanoparticles (Tian et al. 2017). Moreover, the presence of GQDs in TiO_2 has a significant role on the charge recombination as GQDs

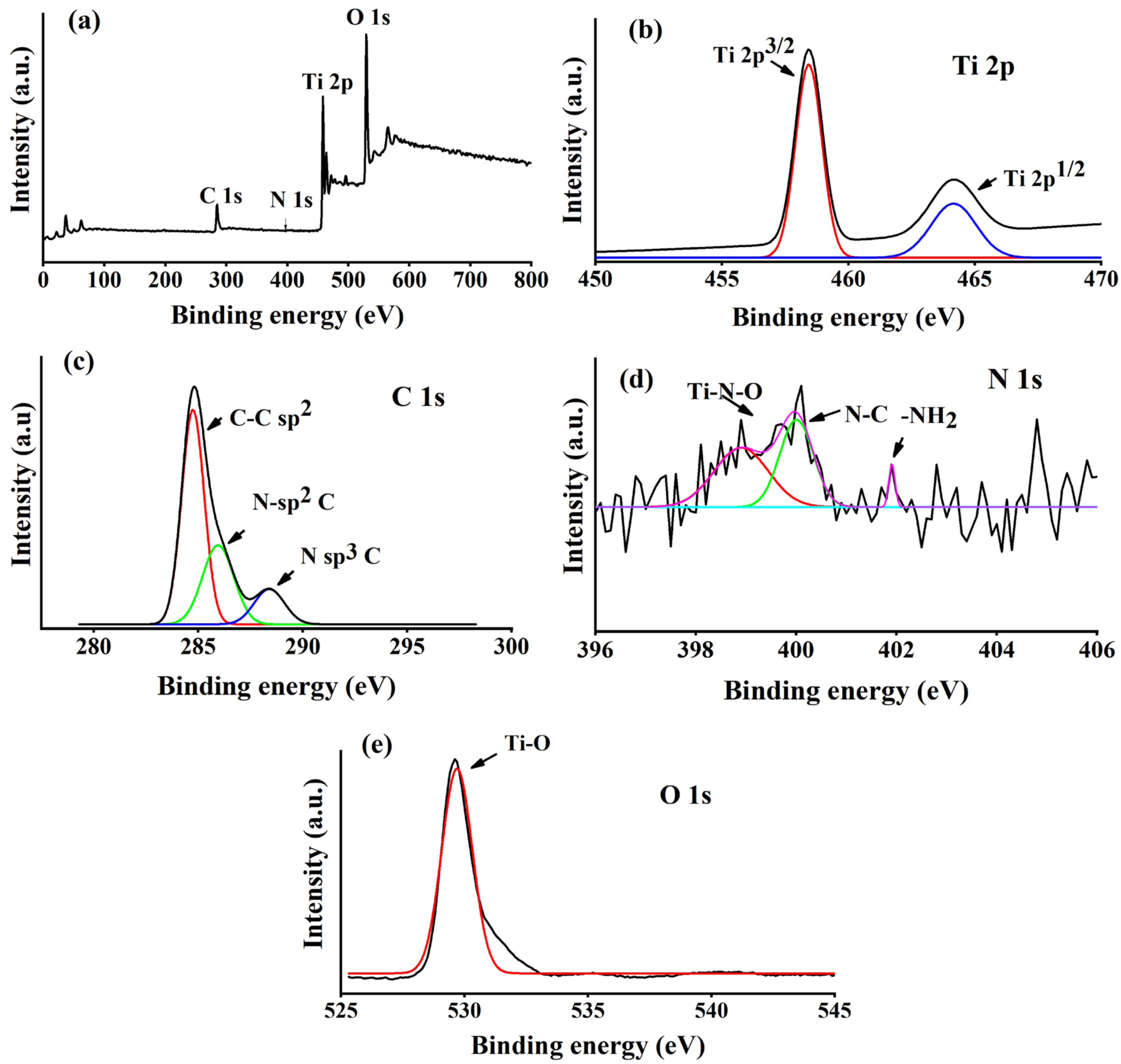

Fig. 5 (**a**) Survey XPS spectrum, (**b**) high-resolution Ti 2p, (**c**) C 1 s, **d** N 1 s, and (**e**) O 1 s spectra of the composite

prevent charge recombination from the conduction band into the valance band, thus facilitates the electron–hole separation at the TiO_2 interface (Ding et al. 2015). In this study, the role of GQDs in prevention of electron–hole recombination is confirmed through PL analysis, where the exciton life is elongated in GQD–20N–TiO_2 compared to TiO_2. The photocatalytic mechanism is discussed in detail in the preceding section.

Effect of photocatalysts dose

Figure 6b shows the photocatalytic activity of different doses of GQD–20N–TiO_2-300 photocatalysts for RB5 photodecolorization ranging from 0.25 to 8 mg/mL, while the other variables were kept constant, i.e., RB5 concentration 30 mg/L, working pH, and temperature 22 ± 2 °C under dark and visible light irradiation to achieve an optimum dose of GQD–20N–TiO_2-300 photocatalyst for RB5 decolorization. The maximum RB5 decolorization was found to be 100% for 1 mg mL^{-1} of GQD–20N–TiO_2-300 dose, while 96% decolorization was observed for 8 mg mL^{-1}. Although the effect on decolorization is lower but this phenomenon can be explained in terms of GQDs presence, as higher concentration of GQDs can adsorb more RB5 molecules but reduce the photocatalytic performance. The increased decolorization attributable to adsorption rather than photodecolorization due to reduced light harvesting, this phenomenon is explained with respect to graphene contents by Tian et al. (Tian et al. 2017).

Effect of pH

Altering the suspension pH can change the surface properties of the photocatalysts. Keeping in view the PZC of

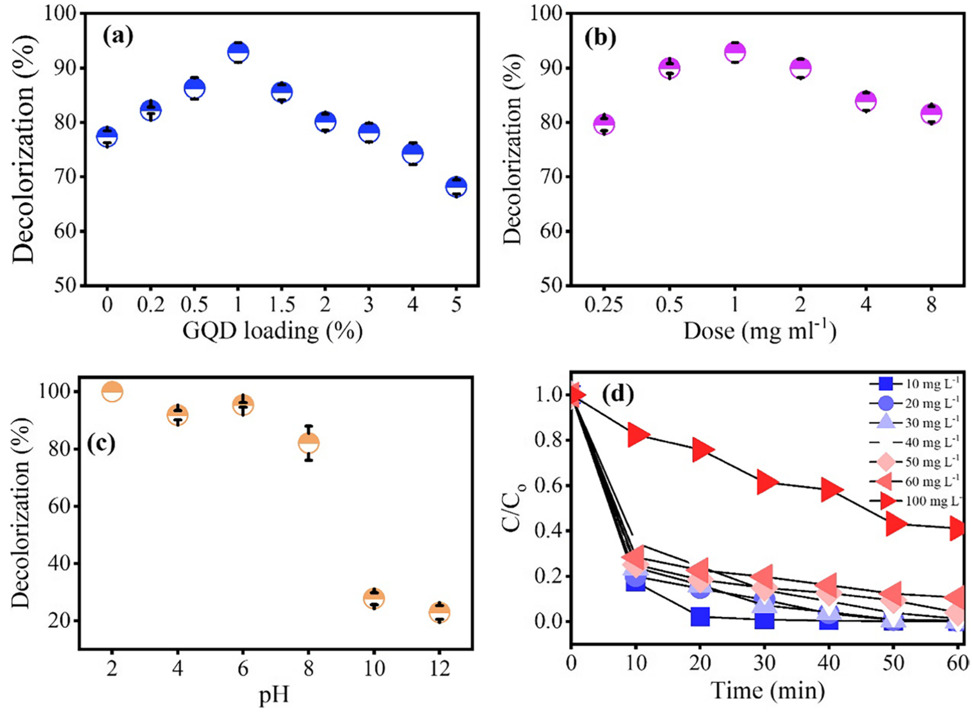

Fig. 6 Effect of different reaction parameters on the decolorization of RB5 dye (**a**) GQDs loading, (**b**) dose (c) pH, and (**d**) initial dye concentration decay profile using GQD–20N–TiO_2-300

TiO_2 (6.28), the TiO_2 surface is positively charged under acidic conditions while negatively charged under basic conditions. These conditions not only affect the surface properties but the redox potential as well as the adsorption capacity of the photocatalyst. Figure 6c shows the effect of varying pH on the decolorization efficiency of the GQD–20N–TiO_2-300 photocatalyst. GQD–20N–TiO_2-300 showed 100, 91, 96, 82, 27, and 22% RB5 dye decolorization at pH 2, 4, 6, 8,10, and 12, respectively. These results demonstrate that lower pH is more favorable for RB5 decolorization as compared to higher pH (Gar Alalm et al. 2015). This phenomenon can be explained by the fact that at lower pH, the protonation takes place, and protonated products are more stable in light as compared to its original molecules. Moreover, as heterogenous photocatalysis is a surface phenomenon and more protonated molecules and anionic dye are attracted towards the surface of GQD–20N–TiO_2-300 photocatalyst surface; hence, more decolorization takes place.

Effect of RB5 concentration

Figure 6d shows the effect of different initial RB5 concentration on percent decolorization efficiency of GQD–20N–TiO_2-300. It can be observed that at the low concentration the percent decolorization was high and the degradation efficiency decreased with increasing initial RB5 concentration. A 95–100% removal was recorded for initial RB5 concentration of 10–40 mg L^{-1} while the efficiency reduced to 60% when dye concentration was 100 mg L^{-1}. The lower efficiency of GQD–20N–TiO_2-300 with increase initial RB5 concentration can be explained by the intensely colored solution upon increasing the initial RB5 concentration and a limited number of active sites availability for the adsorption of dye molecules, this results in lower decolorization efficiency (Jamil et al. 2020). The other reason as explained in previous studies can be the availability of •OH radicles. The number of photons reaching the surface of GQD–20N–TiO_2-300 for excitation decreases as the dye concentration rises, resulting in fewer •OH radicals being generated for RB5 dye decolorization. (Bibi et al. 2017).

Heterogenous photocatalytic kinetic studies

To check the impact of decolorization kinetics different kinetic models, i.e., first, pseudo first- and second-order kinetic models were applied. The plots of first, pseudo first- and second-order kinetic models are depicted in Figure S1 in the supplementary information. Heterogenous photocatalytic kinetic studies for GQDs-doped nitrogen-doped TiO_2 were studied using different initial RB5 dye concentration (Fig. 7). The apparent rate constant (K_{app}) was obtained from pseudo first-order kinetic model and explained in supplementary information (Figure S1 and Table S1). Plot of $1/K_{app}$ versus initial dye concentration was used to describe Langmuir–Hinshelwood model (inset Fig. 7). The photocatalytic decolorization of RB5 by GQD–20N–TiO_2-300 photocatalyst fitted the Langmuir–Hinshelwood model, as

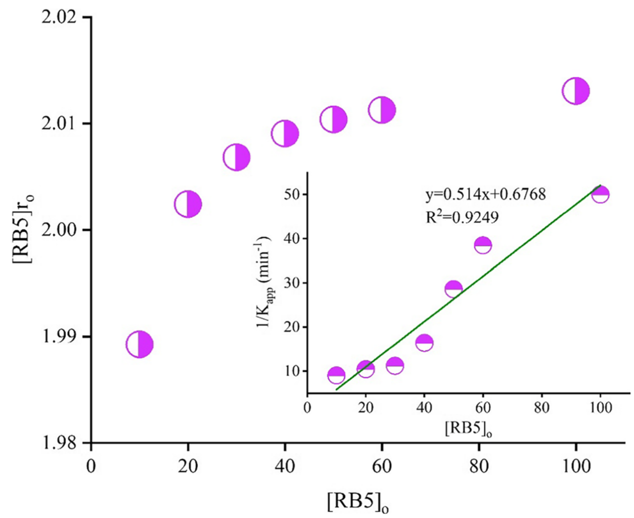

Fig. 7 RB5 degradation rate for different initial RB5 dye concentration, inset plot of reciprocal of apparent rate (K_{app}) of degradation against initial RB5 concentration

illustrated by a linear relationship between the $1/K_{app}$ and initial RB5 dye concentration ($R^2 = 0.9249$). The surface reaction rate constant (K_C) and the adsorption equilibrium constant (K_{LH}) were calculated as $K_C = 1.95$ mg L^{-1} min^{-1} and $K_{LH} = 0.76$ L mg^{-1}, respectively.

Reusability of the photocatalyst

Reusability and recyclability of a photocatalyst are vital from an industrial and economic perspective; however, they have received little attention in recent years. The main aim of heterogenous photocatalysis should be these two aspects. In short, for a photocatalyst to be commercially viable, it must be able to sustain the reaction conditions repeatedly and upon reusing the photocatalyst, the performance must not be significantly altered. Figure 8 shows the recycling studies for TiO_2–300, 20N–TiO_2–300, and GQD–20N–TiO_2–300 photocatalysts up to four cycles. The photocatalytic performance of 20N–TiO_2–300photocatalyst was reduced from 95% in the first cycle to 72% in the fourth cycle while 20N–TiO_2–300photocatalyst showed the performance reduction of 99% in the first cycle to 87% in fourth cycle. Again, the slight decrease in performance can be due to the loss of active sites upon reusing and washing (El-Mekkawi et al. 2020).

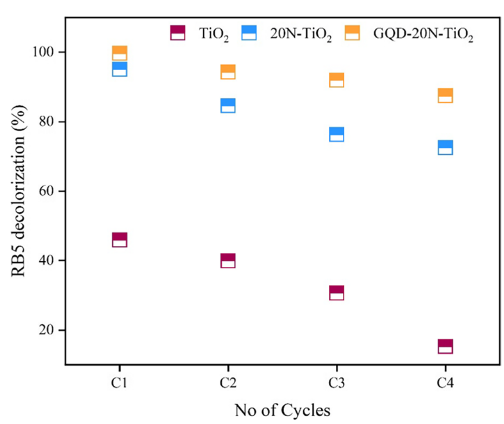

Fig. 8 Reusability studies for TiO_2–300, 20N–TiO_2–300, and GQD–20N–TiO_2–300

Table 1 Comparison of $E_{E/O}$ kWh m^{-3} for the different synthesized photocatalysts

Photocatalyst	$E_{E/O}$ kWh m^{-3}	Reference
0.1Fe–TiO_2–300	207.00	(Khan et al. 2021c)
1Fe–Zn–TiO_2	457	(Riaz et al. 2021)
GQD–0.1Fe–TiO_2–300	137.47	(Khan et al. 2021b)
N–Pt–TiO_2	84.7	(Sun et al. 2013)
GQD–20N–TiO_2–300	89.15	This study

Electrical energy consumption and efficiency

The electrical energy consumed during the removal of RB5 dye from 1000 L of wastewater is depicted in Table 1. The energy consumption of the synthesized photocatalysts was quite lower as compared to the other reported photocatalysts. Moreover, in our previous study, the energy consumption of GQD doped metal doped photocatalysts were 137 k W h m^{-3} (Khan et al. 2021b); however, the nonmetal heterostructure depicted 1.5 time lower energy consumption with GQDs loading in this study.

Photocatalytic mechanism study

The role of electrons, holes, and generation of other reactive species were monitored during the trapping experiments. Based on these findings, a potential reaction mechanism is presented.

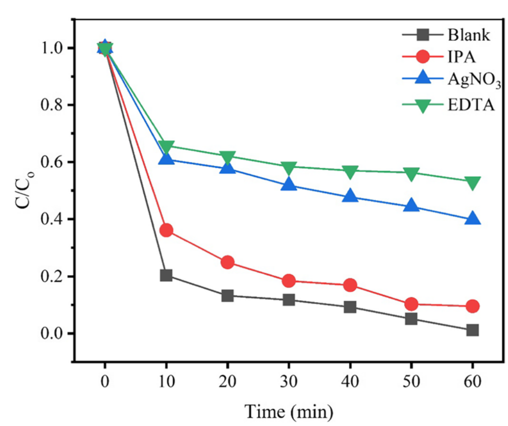

Fig. 9 Proposed photocatalytic mechanism of GQD–20N–TiO_2 for RB5 decolorization

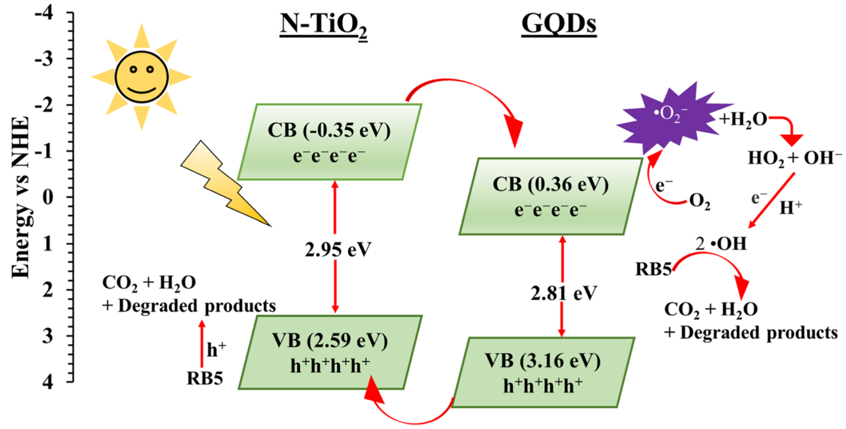

Fig. 10 Effect of different trapping agents on the photocatalytic decolorization of RB5 using GQD–20N–TiO_2–300

The Mulliken electronegativity theory (MET) can be used to compute the conduction (E_{CB}) and valence (E_{VB}) band potentials of 20N-TiO_2 and GQDs to understand the possible reaction processes for RB5 photodecolorization (Eq. 5 and Eq. 6). Figure 9 illustrates the proposed mechanism of 20N-TiO_2 and GQDs for decolorization of RB5 under visible light.

$$E_{CB} = \chi - E^e - 0.5E_g \tag{5}$$

$$E_{VB} = E_{CB} + E_g \tag{6}$$

CB and VB are E_{CB} and E_{VB} potentials, respectively, while E_e is the electrons energy (4.5 eV vs. NHE) (Morrison 1980). The χ (electronegative of the nanocomposite) was determined through the following equation (Eq. 7).

$$\chi = \left[x(A)^a\right]\left[x(B)^b x(B)^b x(C)^c\right]^{\frac{1}{a+b+c}} \tag{7}$$

The compounds' atom counts are denoted by the letters a, b, and c in the equation above (Yuan et al. 2014). The E_{CB}, E_{VB}, and χ of GQDs described in our previous research work were 0.36 eV, 3.16 eV, and 6.26 eV respectively (Khan et al. 2021b). The χ value of N-TiO_2 was estimated to be 5.62 eV and the E_{CB} and E_{VB} were − 0.35 eV and 2.55 eV, respectively. As both N-TiO_2 and GQDs are optically active and can produce electrons and hole pairs, however the photocatalytic activity of N-TiO_2 was recorded higher upon GQDs decoration. When the GQD–N–TiO_2 is subjected to visible light, two possible separation mechanism can occur, i.e., *Z*-scheme and type II heterojunction. In *Z*-scheme, the photoexcited electron on the CB_{GQD} would migrate to the $VB_{N\text{-}TiO2}$, and the photoinduced hole (h +) on the VB_{GQD} (2.59 eV) and the photoexcited electron on the $CB_{N\text{-}TiO2}$ (− 0.35 eV) would subsequently react with H_2O to form hydroxyl radicals (•OH) and superoxide anion radicals (O_2•) (Ma et al. 2019). However, the amount of hydroxyl radicals produced in this study (Fig. 10) is very low, indicating that type II heterojunction is responsible for the photocatalytic RB5 decolorization by GQD–N–TiO_2. In type II heterojunction, electron from the $CB_{N\text{-}TiO2}$ would easily migrate to the CB_{GQD} while the holes in the VB_{GQD} would migrate to the $VB_{N\text{-}TiO2}$ leaving electrons and holes in CB_{GQD} and $VB_{N\text{-}TiO2}$, respectively. Moreover, the production of superoxide (O_2•) is attributed to the reaction at CB_{GQD}. Overall, the photodecolorization reactions are triggered by

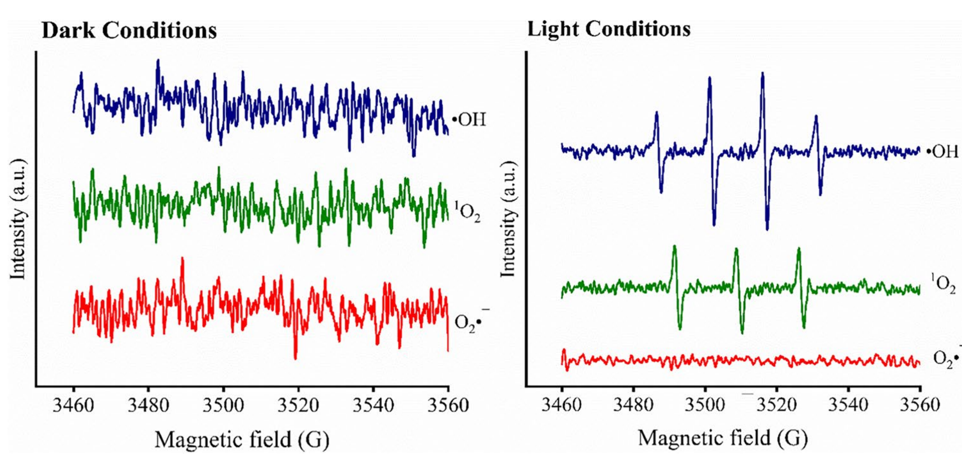

Fig. 11 EPR analysis of the synthesized GQD–20N–TiO_2 photocatalyst in dark and light conditions

the formation of holes and reactive oxygen species on the surface of GQD–N–TiO_2, which react with the adsorbed RB5 molecules.

We further conducted the EPR analysis to demonstrate the presence of reactive oxygen species (ROS) and explain the degradation mechanism of GQD–20N–TiO_2. Figure 11 shows the presence of ROS in GQD–20N–TiO_2 during dark and light conditions. Strong EPR signal were observed during the light conditions compared to dark conditions, which proved that the presence of •OH, $^1O_2$, and O_2• were produced during the photocatalytic process (Gao et al. 2022). These results are consistent with quenching experiment results.

Conclusion

In this study, GQDs were successfully doped on nitrogen-doped TiO_2 with the improved tunable optical properties and desired bandgap for the RB5decolorization. GQDs loading had a significant impact on the performance of 20N–TiO_2 photocatalysts to decolorize RB5. The optimized reaction conditions were 1 g L^{-1} dose, pH 6.8, 60 mg L^{-1} RB5 concentration, and normal room temperature (22 ± 2 °C). The photocatalytic reaction followed the PFO kinetics, and the L–H expression depicted the K_C as 1.95 mg L^{-1} min^{-1} and K_{LH} was 0.76 L mg^{-1}, emphasizing the simultaneous process of adsorption and photocatalysis. Moreover, the physicochemical properties of the best performing material, GQD–20N–TiO_2-300 depicted the elongated exciton lifespan confirmed through reduced PL intensity and E_g (2.91 eV) compared to pristine TiO_2 (E_g = 3.19 eV). The other improved properties were exhibited including surface area (191.91m^2 g^{-1}), pore diameter (1.94 nm), TEM particle size of 4.36 nm, and visibly uniform arrangements and dispersion. XRD results showed consistent anatase even upon introduction of GQDs into 20N-TiO_2 lattice. Furthermore, the decoration of GQDs lowered the Ti 2p XPS spectra to a lower binding energy level (458.36 eV), and binding energy levels of the introduced impurities confirmed the changes in TiO_2 lattice. The proposed mechanism was the type II heterojunction, while the presence of holes and reactive oxygen species were confirmed through EPR analysis, and these species were found to be the main reactive species for the decolorization of RB5 dye. From the economic point of view, GQD–20N–TiO_2 was more durable and energy efficient compared to TiO_2 and 20N-TiO_2 photocatalysts. This study could pave the way for further insight into the photocatalytic behavior of GQDs with other metal oxides for toxic pollutant remediation in environment.

Supplementary Information The online version contains supplementary material available at https://doi.org/10.1007/s11356-023-28782-5.

Author contribution Muhammad Saqib Khan: conceptualization, methodology, investigation, data curation, formal analysis, writing—review and editing. Nadia Riaz, Muhammad Arfan, Ahson Jabbar Shaikh: software, review and editing. Saeed Rahman, Liu Chenhui, Iftikhar Zeb, Farhan Hafeez: formal analysis. Muhammad Arshad, Muhammad Bilal: supervision, conceptualization, resources, funding acquisition, writing—review and editing.

Funding The authors gratefully acknowledge the financial support of the COMSATS University Islamabad Research Grant Program No. (16–79/CRGP/CIIT/ATD/17/1141).

Data availability All data generated or analyzed during this study are included in this article.

Declarations

Ethical approval Not applicable.

Consent to participate Not applicable.

Consent for publication Not applicable.

Competing interests The authors declare no competing interests.

References

Abdullah AM, Al-Thani NJ, Tawbi K, Al-Kandari H (2016) Carbon/nitrogen-doped TiO_2: new synthesis route, characterization and application for phenol degradation. Arab J Chem 9:229–237

Albargi H, Umar A, Shkir M (2021): Enhanced photoresponsivity of anatase titanium dioxide (TiO_2)/nitrogen-doped graphene quantum dots (N-GQDs) heterojunction-based photodetector. Advanced Composites and Hybrid Materials, 1–13

Azami M, Nawawi W, Jawad AH, Ishak M, Ismail K (2017) N-doped TiO_2 synthesised via microwave induced photocatalytic on RR4 dye removal under LED light irradiation. Sains Malaysiana 46:1309–1316

Azbar N, Yonar T, Kestioglu K (2004) Comparison of various advanced oxidation processes and chemical treatment methods for COD and color removal from a polyester and acetate fiber dyeing effluent. Chemosphere 55:35–43

Bibi I, Nazar N, Iqbal M, Kamal S, Nawaz H, Nouren S, Safa Y, Jilani K, Sultan M, Ata S, Rehman F, Abbas M (2017) Green and eco-friendly synthesis of cobalt-oxide nanoparticle: characterization and photo-catalytic activity. Adv Powder Technol 28:2035–2043

Bruce JA, Clapper JC (2020) Conjugation of carboxylated graphene quantum dots with cecropin P1 for bacterial biosensing applications. ACS Omega 5:26583–26591

Chambers SA (2016): Probing perovskite interfaces and superlattices with X-ray photoemission spectroscopy, Hard X-ray photoelectron spectroscopy (HAXPES). Springer, pp. 341–380

Chang Z, Zhang C, Yao B (2021): Novel dual-sensitization electrochemiluminescence immunosensor using photopermeable Ru $(bpy)_3^{2+}$-doped chitosan/SiO_2 nanoparticles as labels and chitosan-decorated Nafion/MWNTs composites as enhancer. Luminescence

Chen F, Liu L-L, Zhang Y-J, Wu J-H, Huang G-X, Yang Q, Chen J-J, Yu H-Q (2020) Enhanced full solar spectrum photocatalysis by nitrogen-doped graphene quantum dots decorated BiO_2-x nanosheets: ultrafast charge transfer and molecular oxygen activation. Appl Catal B 277:119218

Cheng G, Liu X, Song X, Chen X, Dai W, Yuan R, Fu X (2020) Visible-light-driven deep oxidation of NO over Fe doped TiO_2

catalyst: synergic effect of Fe and oxygen vacancies. Appl Catal B 277:119196

Ding Z, Hao Z, Meng B, Xie Z, Liu J, Dai L (2015) Few-layered graphene quantum dots as efficient hole-extraction layer for high-performance polymer solar cells. Nano Energy 15:186–192

Dong Y, Shao J, Chen C, Li H, Wang R, Chi Y, Lin X, Chen G (2012) Blue luminescent graphene quantum dots and graphene oxide prepared by tuning the carbonization degree of citric acid. Carbon 50:4738–4743

El-Mekkawi DM, Abdelwahab NA, Mohamed WAA, Taha NA, Abdel-Mottaleb MSA (2020) Solar photocatalytic treatment of industrial wastewater utilizing recycled polymeric disposals as TiO_2 supports. J Clean Prod 249:119430

Factorovich M, Guz L, Candal R (2011) N-TiO_2: chemical synthesis and photocatalysis. Advances in Physical Chemistry 2011:1–8

Ganganboina AB, Chowdhury AD, Doong R-a (2017) Nano assembly of N-doped graphene quantum dots anchored Fe_3O_4/halloysite nanotubes for high performance supercapacitor. Electrochim Acta 245:912–923

Gao X, Li Q, Zhu W, Li X, Guo Y (2022) N, S co-doped graphene quantum dots promote charge separation of Bi4O5BrxI2−x solid solution and enhance visible light photocatalytic performance. Colloids Surf, A 648:129155

Gar Alalm M, Tawfik A, Ookawara S (2015) Comparison of solar TiO_2 photocatalysis and solar photo-Fenton for treatment of pesticides industry wastewater: operational conditions, kinetics, and costs. Journal of Water Process Engineering 8:55–63

Gómez IJ, VázquezSulleiro M, Dolečková A, Pizúrová N, Medalová J, Roy R, Nečas D, Zajíčková L (2021) Exploring the emission pathways in nitrogen-doped graphene quantum dots for bioimaging. The Journal of Physical Chemistry C 125:21044–21054

Guo Z, Wu H, Li M, Tang T, Wen J, Li X (2020) Phosphorus-doped graphene quantum dots loaded on TiO_2 for enhanced photodegradation. Appl Surf Sci 526:146724

Iftikhar A, Khan MS, Rashid U, Mahmood Q, Zafar H, Bilal M, Riaz N (2020): Influence of metallic species for efficient photocatalytic water disinfection: bactericidal mechanism of in vitro results using docking simulation. Environmental Science and Pollution Research

Jamil A, Bokhari TH, Javed T, Mustafa R, Sajid M, Noreen S, Zuber M, Nazir A, Iqbal M, Jilani MI (2020) Photocatalytic degradation of disperse dye Violet-26 using TiO_2 and ZnO nanomaterials and process variable optimization. J Market Res 9:1119–1128

Jiang Z, Lei Y, Zhang Z, Hu J, Lin Y, Ouyang Z (2020) Nitrogen-doped graphene quantum dots decorated ZnxCd1-xS semiconductor with tunable photoelectric properties. J Alloy Compd 812:152096

Kang X, Chaperman L, Galeckas A, Ammar S, Mammeri F, Norby T, Chatzitakis A (2021) Water vapor photoelectrolysis in a solid-state photoelectrochemical cell with TiO2 nanotubes loaded with CdS and CdSe nanoparticles. ACS Appl Mater Interfaces 13:46875–46885

Khan MS, Shah JA, Arshad M, Halim SA, Khan A, Shaikh AJ, Riaz N, Khan AJ, Arfan M, Shahid M, Pervez A, Aa H, Bilal M (2020) Photocatalytic decolorization and biocidal applications of nonmetal doped TiO_2: isotherm, kinetic modeling and In Silico molecular docking studies. Molecules 25:4468

Khan MS, García MF, Javed M, Kubacka A, Caudillo-Flores U, Halim SA, Khan A, Al-Harrasi A, Riaz N (2021a) Synthesis, characterization, and photocatalytic, bactericidal, and molecular docking analysis of Cu–Fe/TiO_2 photocatalysts: influence of metallic impurities and calcination temperature on charge recombination. ACS Omega 6:26108–26118

Khan MS, Riaz N, Shaikh AJ, Shah JA, Hussain J, Irshad M, Awan MS, Syed A, Kallerhoff J, Arshad M, Bilal M (2021b) Graphene quantum dot and iron co-doped TiO_2 photocatalysts: synthesis, performance evaluation and phytotoxicity studies. Ecotoxicol Environ Saf 226:112855

Khan MS, Shah JA, Riaz N, Butt TA, Khan AJ, Khalifa W, Gasmi HH, Latifee ER, Arshad M, Al-Naghi AAA, Ul-Hamid A, Arshad M, Bilal M (2021c) Synthesis and characterization of Fe-TiO_2 Nanomaterial: performance evaluation for RB5 decolorization and in vitro antibacterial studies. Nanomaterials 11:436

Khore SK, Kadam SR, Naik SD, Kale BB, Sonawane RS (2018) Solar light active plasmonic Au@TiO_2 nanocomposite with superior photocatalytic performance for H_2 production and pollutant degradation. New J Chem 42:10958–10968

Khorshidi E, Rezaei B, Irannejad N, Adhami S, Ebrahimi M, Kermanpur A, Ensafi AA (2020) The role of GQDs additive in TiO_2 nanorods as an electron transfer layer on performance improvement of the perovskite solar cells. Electrochim Acta 337:135822

Koe WS, Chong WC, Pang YL, Koo CH, Ebrahim M, Mohammad AW (2020) Novel nitrogen and sulphur co-doped carbon quantum dots/titanium oxide photocatalytic membrane for in-situ degradation and removal of pharmaceutical compound. Journal of Water Process Engineering 33:101068

Lei Y, Wu Y, Jiang Z, Ouyang Z, Hu J, Lin Y, Du P, Zou B (2021) Effect of various mass ratios of graphene quantum dots doping on the photoelectric performance of ZnSe-GQDs nanocomposites. Mater Sci Semicond Process 128:105740

Li Y, Zhao Y, Cheng H, Hu Y, Shi G, Dai L, Qu L (2012) Nitrogen-doped graphene quantum dots with oxygen-rich functional groups. J Am Chem Soc 134:15–18

Lu D, Zhang M, Zhang Z, Li Q, Wang X, Yang J (2014) Self-organized vanadium and nitrogen co-doped titania nanotube arrays with enhanced photocatalytic reduction of CO_2 into CH_4. Nanoscale Res Lett 9:1–9

Ma R, Zhang S, Li L, Gu P, Wen T, Khan A, Li S, Li B, Wang S, Wang X (2019) Enhanced visible-light-induced photoactivity of type-II CeO_2/g-C_3N_4 nanosheet toward organic pollutants degradation. ACS Sustainable Chemistry & Engineering 7:9699–9708

Mahalingam S, Manap A, Omar A, Low FW, Afandi N, Chia CH, Abd Rahim N (2021) Functionalized graphene quantum dots for dye-sensitized solar cell: key challenges, recent developments and future prospects. Renew Sustain Energy Rev 144:110999

Mahato D, Kharwar YP, Ramanujam K, Haridoss P, Thomas T (2021) S, N co-doped graphene quantum dots decorated TiO_2 and supported with carbon for oxygen reduction reaction catalysis. Int J Hydrogen Energy 46:21549–21565

Martins NCT, Ângelo J, Girão AV, Trindade T, Andrade L, Mendes A (2016) N-doped carbon quantum dots/TiO_2 composite with improved photocatalytic activity. Appl Catal B 193:67–74

Miodyńska M, Mikolajczyk A, Bajorowicz B, Zwara J, Klimczuk T, Lisowski W, Trykowski G, Pinto HP, Zaleska-Medynska A (2020) Urchin-like TiO_2 structures decorated with lanthanide-doped Bi_2S_3 quantum dots to boost hydrogen photogeneration performance. Appl Catal B 272:118962

Miranda-Andrades JR, Letichevsky S, Larrudé DRG, Aucelio RQ (2020) Photo-generation of mercury cold vapor mediated by graphene quantum dots/TiO_2 nanocomposite: on line time-resolved speciation at ultra-trace levels. Anal Chim Acta 1127:256–268

Morrison SR (1980): Electrochemistry at semiconductor and oxidized metal electrodes, United States

Pan D, Jiao J, Li Z, Guo Y, Feng C, Liu Y, Wang L, Wu M (2015) Efficient separation of electron–hole pairs in graphene quantum dots by TiO_2 heterojunctions for dye degradation. ACS Sustainable Chemistry & Engineering 3:2405–2413

Peñas-Garzón M, Abdelraheem WHM, Belver C, Rodriguez JJ, Bedia J, Dionysiou DD (2021) TiO_2-carbon microspheres as photocatalysts for effective remediation of pharmaceuticals under simulated solar light. Sep Purif Technol 275:119169

Pourzad A, Sobhi HR, Behbahani M, Esrafili A, Kalantary RR, Kermani M (2020) Efficient visible light-induced photocatalytic

removal of paraquat using N-doped TiO_2@ SiO_2@ Fe_3O_4 nanocomposite. J Mol Liq 299:112167
Riaz N, Chong FK, Dutta BK, Man ZB, Khan MS, Nurlaela E (2012) Photodegradation of Orange II under visible light using Cu-Ni/TiO_2: effect of calcination temperature. Chem Eng J 185:108–119
Riaz N, Kait CF, Man Z, Dutta BK, Ramli RM, Khan MS (2014) Visible light photodegradation of azo dye by Cu/TiO_2. Advanced Materials Research 917:151–159
Riaz N, Fen DACS, Khan MS, Naz S, Sarwar R, Farooq U, Bustam MA, Batiha GE-S, El Azab IH, Uddin J, Khan A (2021) Iron-zinc co-doped titania nanocomposite: photocatalytic and photobiocidal potential in combination with molecular docking studies. Catalysts 11:1112
Sadhasivam S, Gunasekaran A, Anbarasan N, Mukilan N, Jeganathan K (2021): CdS and CdSe nanoparticles activated 1D TiO2 heterostructure nanoarray photoelectrodes for enhanced photoelectrocatalytic water splitting. International Journal of Hydrogen Energy
Saha NC, Tompkins HG (1992) Titanium nitride oxidation chemistry: an x-ray photoelectron spectroscopy study. J Appl Phys 72:3072–3079
Shabir M, Shezad N, Shafiq I, Maafa IM, Akhter P, Azam K, Ahmed A, Lee SH, Park Y-K, Hussain M (2021): Carbon nanotubes loaded N,S-codoped TiO_2: heterojunction assembly for enhanced integrated adsorptive-photocatalytic performance. Journal of Industrial and Engineering Chemistry
Shah H, Xie W, Wang Y, Jia X, Nawaz A, Xin Q, Song M, Gong JR (2021) Preparation of blue- and green-emissive nitrogen-doped graphene quantum dots from graphite and their application in bioimaging. Mater Sci Eng, C 119:111642
Stankovich S, Piner RD, Nguyen ST, Ruoff RS (2006) Synthesis and exfoliation of isocyanate-treated graphene oxide nanoplatelets. Carbon 44:3342–3347
Sun H, Zhou G, Liu S, Ang HM, Tadé MO, Wang S (2013) Visible light responsive titania photocatalysts codoped by nitrogen and metal (Fe, Ni, Ag, or Pt) for remediation of aqueous pollutants. Chem Eng J 231:18–25
Sun X, Li H-J, Ou N, Lyu B, Gui B, Tian S, Qian D, Wang X, Yang J (2019) Visible-light driven TiO_2 Photocatalyst coated with graphene quantum dots of tunable nitrogen doping. Molecules 24:344
Tian H, Shen K, Hu X, Qiao L, Zheng W (2017) N, S co-doped graphene quantum dots-graphene-TiO_2 nanotubes composite with enhanced photocatalytic activity. J Alloy Compd 691:369–377
Upadhyay GK, Rajput JK, Pathak TK, Pal PK, Purohit LP (2020) Tailoring and optimization of hybrid ZnO:TiO_2:CdO nanomaterials for advance oxidation process under visible light. Appl Surf Sci 509:145326
Wu H, Ding J, Yang D, Li J, Shi Y, Zhou Y (2020) Graphene quantum dots doped ZnO superstructure (ZnO superstructure/GQDs) for weak UV intensity photodetector application. Ceram Int 46:17800–17808
Xue H, Jiang Y, Yuan K, Yang T, Hou J, Cao C, Feng K, Wang X (2016) Floating photocatalyst of B-N–TiO_2/expanded perlite: a sol–gel synthesis with optimized mesoporous and high photocatalytic activity. Sci Rep 6:1–9
Yang J, Miao H, Jing J, Zhu Y, Choi W (2021) Photocatalytic activity enhancement of PDI supermolecular via π-π action and energy level adjusting with graphene quantum dots. Appl Catal B 281:119547
Yoon H, Kim HS, Kim J, Park M, Kim B, Lee S, Kang K, Yoo S, Jeon S (2020) Blue graphene quantum dots with high color purity by controlling subdomain formation for light-emitting devices. ACS Applied Nano Materials 3:6469–6477
Yuan Q, Chen L, Xiong M, He J, Luo S-L, Au C-T, Yin S-F (2014) Cu_2O/BiVO4 heterostructures: synthesis and application in simultaneous photocatalytic oxidation of organic dyes and reduction of Cr(VI) under visible light. Chem Eng J 255:394–402
Zheng L, Su H, Zhang J, Walekar LS, Molamahmood HV, Zhou B, Long M, Hu YH (2018) Highly selective photocatalytic production of H_2O_2 on sulfur and nitrogen co-doped graphene quantum dots tuned TiO_2. Appl Catal B 239:475–484
Zhou L, Cai M, Zhang X, Cui N, Chen G, Zou G-y (2020) In-situ nitrogen-doped black TiO_2 with enhanced visible-light-driven photocatalytic inactivation of Microcystis aeruginosa cells: synthesization, performance and mechanism. Appl Catal B 272:119019

Authors and Affiliations

Muhammad Saqib Khan[1,2] · Nadia Riaz[1] · Saeed Rehman[3] · Liu Chenhui[3] · Ahson Jabbar Shaikh[4] · Muhammad Arfan[5] · Iftikhar Zeb[6] · Muhammad Arshad[7] · Farhan Hafeez[1] · Muhammad Bilal[1]

✉ Muhammad Bilal
mbilal@cuiatd.edu.pk

[1] Department of Environmental Sciences, COMSATS University Islamabad, Abbottabad Campus, Abbottabad 22060, Pakistan

[2] Department of Biomedical Sciences, Pak-Austria Fachhochschule: Institute of Applied Sciences and Technology, Mang, Khanpur Road, Haripur 22621, KPK, Pakistan

[3] School of Environment and Energy, South China University of Technology, Guangzhou 510006, China

[4] Department of Chemistry, COMSATS University Islamabad, Abbottabad Campus, Abbottabad Campus, Abbottabad 22060, Pakistan

[5] Department of Chemistry, School of Natural Sciences, National University of Sciences and Technology, Islamabad 44000, Pakistan

[6] Department of Biotechnology, COMSATS University Islamabad, Abbottabad Campus, Abbottabad 22060, Pakistan

[7] Institute of Environmental Sciences and Engineering, School of Civil and Environmental Engineering, National University of Sciences and Technology, Islamabad 44000, Pakistan